# Experimental investigation of ventilated supercavitation under unsteady conditions

[1, 2]Siyao Shao; [1]Yue Wu; [1, 2]Joseph Haynes; [1,2]Roger Arndt; [1,2]Jiarong Hong*

[1]*Saint Anthony Falls Laboratory, University of Minnesota, Minneapolis, MN, USA;* [2]*Department of Mechanical Engineering, University of Minnesota, Minneapolis, MN, USA*

## Abstract

Ventilated supercavitation is a promising technique to achieve high-speed transport underwater by generating a gas bubble enclosing a moving object through ventilation. However, implementing this technique requires clear understanding and precise control of supercavity behaviors under unsteady conditions in practical applications. In this study, we present the systematic investigation of ventilated supercavity behaviors over a broad range of unsteady conditions. The experiments are conducted in the high-speed water tunnel at Saint Anthony Falls Laboratory. The unsteady conditions are generated using a gust generator consisting of two flapping hydrofoils mounted upstream of a forward-facing cavitator. We use high-speed imaging to capture the variation of cavity dimension and flow patterns along with simultaneous pressure measurements. Measurements are conducted under fixed tunnel speed and ventilation rate with the flapping hydrofoils operating under varying angle of attack (*AoA*) and frequency ($f_g$). The visualization and pressure signals reveal five distinct states of supercavity under unsteady conditions, referred to as stable state, wavy state, pulsating state I, pulsating state II and collapsing state. The stable state occurs under low *AoA* and $f_g$, the supercavity only exhibits small amplitude of oscillation without appreciable deformation of the cavity interface. When the supercavity is at wavy state (moderate *AoA* and high $f_g$), the supercavity displays clear periodic wavelike deformation of its surface with cavity pressure varies periodically at two times of $f_g$. Under high *AoA* with low $f_g$, pulsating state I of the cavity shows significant fluctuations in length with intermittent shed-off of gas pockets at the rear part of the cavity. With increase of $f_g$, the cavity exhibits enhanced pulsating behavior and a sharp of difference between cavity pressure and test section pressure (i.e. pulsating state II). At the highest *AoA* (i.e. *AoA* 10°) and $f_g$ above 2 Hz, the cavity collapses. The transition across different supercavity states under a broad range of unsteady conditions is summarized in the supercavity state map, showing the dependence of supercavity states on the characteristic scales of unsteadiness in comparison to longitudinal and lateral dimensions of the supercavity.

**Keywords**: ventilated supercavitation; unsteady flow; flow instability

## Introduction

Ventilated supercavitation, i.e., a special form of cavitation in which the bubble created by injecting non-condensable gas envelopes the entire underwater object, has gained considerable research attention as a promising way to achieve high speed underwater transportation **[1]**. Conventionally, this phenomenon has been characterized using several non-dimensional parameters, including cavitation number, $\sigma = 2(P_\infty - P_c)/(\rho_w U^2)$, Froude number, $Fr = U/\sqrt{g d_c}$, and air entrainment coefficient, $C_Q = Q/U d_c^2$, where $P_\infty$ and $P_c$ refer to the test-section pressure upstream of the cavitator and the cavity pressure, respectively, $\rho_w$ corresponds to liquid density, $U$ is the free-stream velocity, $g$ refers to the gravitational acceleration, $d_c$ denotes the cavitator diameter, and $Q$ is the volumetric ventilation rate (Notes that in our study we use the volumetric air flow rate under standard condition, i.e, $Q_{As}$, to define air entrainment coefficient $C_{Qs}$) . In practical applications, the operation of a supercavitating object faces unavoidable unsteady conditions, associated with the motions of the object as well as the variation of incoming flows due to changing in depth or surface waves, which could potentially destabilize the supercavity and adversely impact the motion of the object. Therefore, it is necessary to investigate the fundamental physics dictating the behavior of ventilated supercavity in unsteady flows in order to provide guidelines for controlling supercavitating objects under practical operational conditions. However, up to now, there is only handful of investigations in this area **[2-6],** and no systematic experimental studies have been conducted. Logvinovich first proposed supercavity independency theory for the variation of cavity geometry in unsteady flows, i.e., every lateral section of a cavity expands relative to the trajectory of the body center almost independent of the prior or the subsequent body movement, depending only on pressure and velocity at the current moment **[2]**. Based on experiments and numerical simulation, Sememenko provided some observation of supercavity behaviors (e.g., cavity pulsating, closure variation, cavity surface waves etc.) under unsteady conditions with no systematic parameterization and in-depth analysis of flow physics **[3].** Recently, using a

*Corresponding Author, Jiarong Hong: jhong@umn.edu

gust generator in high-speed water tunnel at the Saint Antony Falls Laboratory (SAFL), Lee et al. **[4]** investigated the periodic variation of cavity geometry under a narrow range of unsteady flow conditions. With the same setup, Karn et al. investigated the closure variation for one cavitator (10 mm in diameter) under two specific gust frequencies **[5]** as well as the ventilation demand for the formation and sustenance of a supercavity under similar unsteady flows **[6]**. Following up these prior studies **[4-6]**, here we present the first systematic investigation of the behavior of ventilated supercavity over a broad range of unsteady conditions. In the following sections, we provide a summary of our experimental methodology, the results showing distinct supercavity states obtained under different unsteady conditions, and the analysis of the mechanisms governing the occurrence of each supercavity state. A cavity state map summarizing the transition across different states will also be presented and followed by a conclusion.

## Methodology

The experiments are conducted in the SAFL high-speed water tunnel. The tunnel has been used for a number of supercavitation experiments in recent years [**5-9**]. A forward-facing cavitator mounted on a ventilation pipe (FFM) is employed to generate a stable ventilated supercavity with clear interface. As shown in figure 1(a), the unsteady conditions are introduced using a gust generator consisting of two parallel NACA0020 flapping hydrofoils mounted upstream of the cavitator. The hydrofoils have a chord length of 40 mm, driven by an eccentricity flywheel via pivot arms. The pivot arms apply the periodic pitching motion to the hydrofoils, which allows the hydrofoils flapping in phase to generate a periodic flow inside the water tunnel (details provided in **[10]**). We use high speed imaging to capture the variation of supercavity dimension and flow patterns along with simultaneous measurements of the test section and the cavity pressure. Specifically, high speed imaging is performed with a Photron APX-RS high speed camera with a full resolution of 1k×1k pixels up to 3000 fps. The test section pressure is recorded at one location slightly upstream of the gust generator using Validyne AP 10-50 absolute pressure transducer. The cavity pressure ($P_c$) is derived by monitoring the pressure difference between the test section ($P_\infty$) and one location inside the supercavity ($\Delta P$) using Validyne DP 15-38 differential pressure transducer. Both pressure measurements are obtained at a sampling frequency of 1 kHz with uncertainty ± 100 Pa. The ventilated supercavity is generated using a cavitator of 10 mm in diameter with air ventilation at 10 SLPM (i.e., liter per minute of gas under standard condition) at a fixed flow speed of 8.2 m/s. During the experiments, the flapping hydrofoils of the gust generator are operated under angle of attack ($AoA$) of ±2º, ±4º, ±8º, ±10º and frequency ($f_g$) of 1 Hz, 1.5 Hz, 2 Hz, 3 Hz, 5 Hz, 6 Hz and 10 Hz. As shown in figure 1(b), the perturbation produced from the gust generator can be characterized with its wavelength, $\lambda = U/f_g$ and wave amplitude, $\varepsilon = V_{max}/2\pi f_g$, where the $V_{max}$ denotes the maximum vertical speed of the gust under different $AoA$s and $f_g$ **[4, 10, 11]**. In each gust cycle, there are two maximum perturbations induced by the hydrofoils passing when they move from their neutral position upwards and downwards, respectively. It is worth noting that for a gust of frequency $f_g$, the frequency of test section pressure variation occurs at $2f_g$ and 90º out of phase with respect to the maximum vertical perturbation induced by the moving hydrofoils.

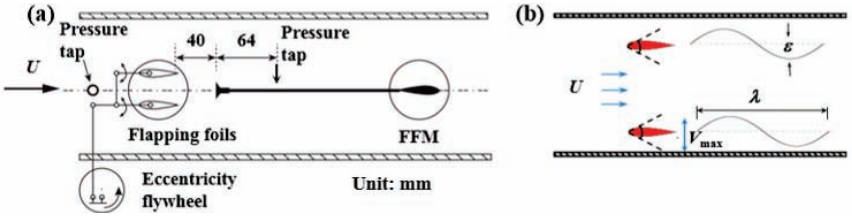


Figure 1. Schematics showing (a) the experimental setup and (b) the wavelength and amplitude of perturbation produced by the gust generator.

## Results

The high-speed visualization and pressure signals reveal five distinct states of the supercavity under unsteady conditions, referred to as stable state, wavy state, pulsating state I, pulsating state II and collapsing state hereafter. The stable state cavity is observed under low $AoA$ and $f_g$. As shown in figure 2(a), the supercavity only exhibits very small amplitude of oscillation without appreciable deformation of the cavity surface. Correspondingly, the variation of the pressure difference ($\Delta P$) fluctuates irregularly at amplitudes equivalent to the noise level of the pressure transducer. Further, power density spectrum (PSD) of $\Delta P$ (not shown for brevity) does not show any peaks near the $f_g$. Overall,

at stable state cavity, the perturbation introduced by flow unsteadiness is not strong enough to cause appreciable change of supercavity behavior.

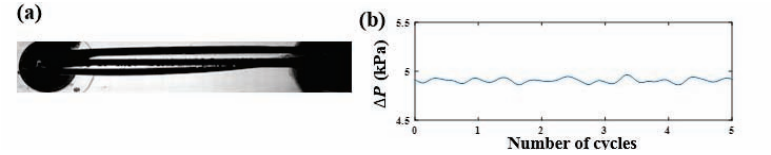


Figure 2. (a) A snapshot of the supercavity and (b) the variation of pressure difference between test section and the cavity ($\Delta P$) at stable state.

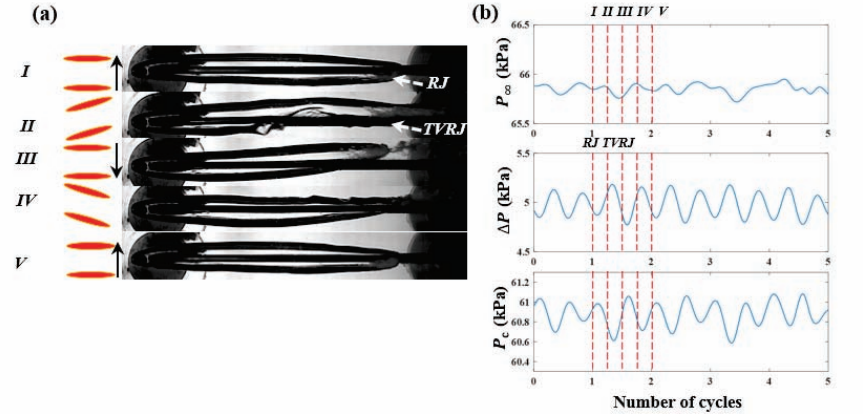


Figure 3. (a) Snapshots showing different phases of supercavity pattern corresponding to different hydrofoil positions in a gust cycle and (b) variation of pressure in test section ($P_\infty$ ), pressure difference between test section and the cavity ($\Delta P$) and cavity pressure ($P_c$) derived from $P_\infty$ and $\Delta P$ at wavy state. The arrows in (a) indicate the motion of hydrofoils.

The wavy state occurs under moderate *AoA* and high $f_g$. The supercavity displays clear periodic wavelike undulation at its surface with a variation of closure types between re-entrant jet (RJ) and a hybrid mode of twin vortex (TV) and RJ (TVRJ) (figure 3(a)). Accordingly, as shown in figure 3(b), the $\Delta P$ and the $P_c$ exhibit periodic variation with double peaks in each gust cycle. Particularly, the two peaks in $P_c$ correspond to the two neural positions (i.e., *AoA*=0º, Phases ***I*** and ***III*** in the figure) of the flapping foils with a slight delay of 0.014 s matching the time required for the flow disturbance to propagate from the gust generator to the cavity pressure measurement port. Specifically, as the flapping foils start from their neutral position and move upwards (Phase ***I***), the foils have their maximum vertical velocity leading to the maximum vertical perturbation in a gust cycle. At this phase, the total loss in the water tunnel is the minimum in a gust cycle, leading to the highest tunnel velocity and local minimum of the test section pressure upstream of the gust generator. According to **[5]**, the pressure on the downstream side of the supercavity is high in the gust cycle, contributing the RJ closure mode. The maximum perturbation from the hydrofoils propagates downstream and reaches to the pressure measurement port of the cavity, causing a local maximum in the cavity pressure with 0.014 s delay. As foils moves towards their maximum upward position (Phase ***II***), the total loss in the tunnel rises, leading to a decrease of tunnel velocity and an increase of the test section pressure. Correspondingly, the perturbation from the hydrofoils causes the cavity pressure to drop from its maximum, and consequently the cavity closure transitions from RJ to TVRJ. In addition, the cavity surface deformation and the bubble shed-off from the interface due to Kevin-Helmholtz (KH) instability can be clearly observed. When the foils move downward back to their neutral location (Phase ***III***), the total loss in the tunnel decreases and the test section pressure increases accordingly. The cavity pressure begins to increase and reaches the second peak in a cycle with the same time delay as the one mentioned before. Accordingly, the closure mode shifts back to RJ from TVRJ. As the foils continue to move downwards from its neutral location (***III***), the trends of pressure variation and closure change are similar to those when the foils move from Phase ***I*** to ***II***, and the wavelike undulation of the surface occurs in an opposite phase compared to that during Phase ***I*** to ***II***.

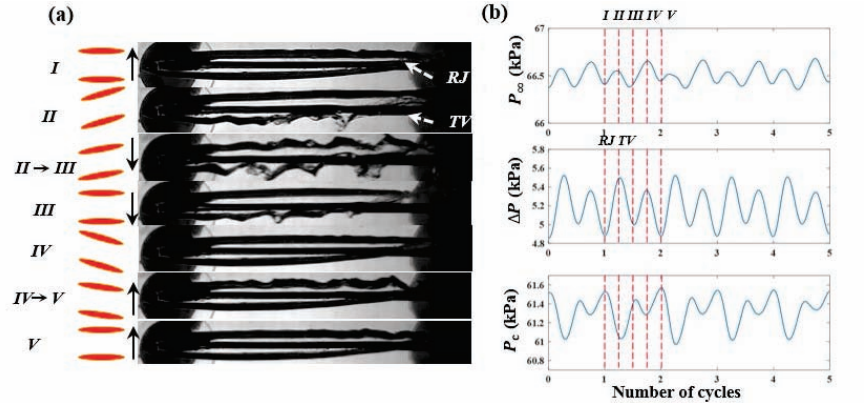


Figure 4. (a) Snapshots showing different phases of supercavity pattern corresponding to different hydrofoil positions in a gust cycle and (b) variation of $P_\infty$ , $\Delta P$ and $P_c$ derived from $P_\infty$ and $\Delta P$ at pulsating state I. The arrows in (a) indicate the motion of hydrofoils.

Pulsating state I is observed under high $AoA$ and low $f_g$. The supercavity exhibits pulsating behavior, i.e., intermittent shed-off of gas pockets at the rear part of the cavity leading to significant fluctuation in length. As shown in figure 4(a), this process is also accompanied with wavelets generating on the cavity surfaces and the variation of closure type between TV and RJ. Due to the relatively weak vertical perturbation associated with the gust generator operating at low $f_g$, the supercavity at this state does not have a wavy deformation on cavity surfaces, different from that of the wavy state. Additionally, the $\Delta P$ and the corresponding $P_c$ exhibits periodic variation with double peaks in each gust cycle, and the two peaks in $\Delta P$ (i.e., local minima of $P_c$) coincide with the timing of the bubble pockets shed-off when the flapping foils reach maximum $AoA$. In comparison to wavy state, as the hydrofoils change in a gust cycle, both the test section pressure and supercavity closure yield similar trends. However, unlike wavy state, the variation of $\Delta P$ and $P_c$ at this stage is primarily dictated by the pressure fluctuation associated with the periodic variation of hydrofoil blockage. The propagation of such pressure fluctuation occurs at the speed of sound in water, significantly faster than the convection speed of vertical velocity perturbation induced by the hydrofoils. Therefore, little delay is observed between the phase change of hydrofoils and the signals of $\Delta P$ and $P_c$. Moreover, the increasing $AoA$ of flapping foils (compared to the wave state) leads to stronger fluctuations of $\Delta P$ and $P_c$, which further induces significant cavity length fluctuations. Particularly, during the transition from Phases ***II*** to ***III*** and from Phases ***IV*** to ***V*** (corresponding to ***II→III*** and ***IV→V*** in figure 4(a), respectively), the cavity length shrinks drastically, resulting in enhanced KH instability and consequently the formation of clear wavelets on the cavity surface. It is also worth noting that the wavelet formation appears to be more dramatic during ***II→III*** compared to ***IV→V*** since the gravity is aligned with downward of the hydrofoils**.** In addition, during the pulsating state I, the closure transitions from RJ to TV, instead of TVRJ in the wavy state, due to the higher tunnel loss caused by the gust generator operated at higher $AoA$.

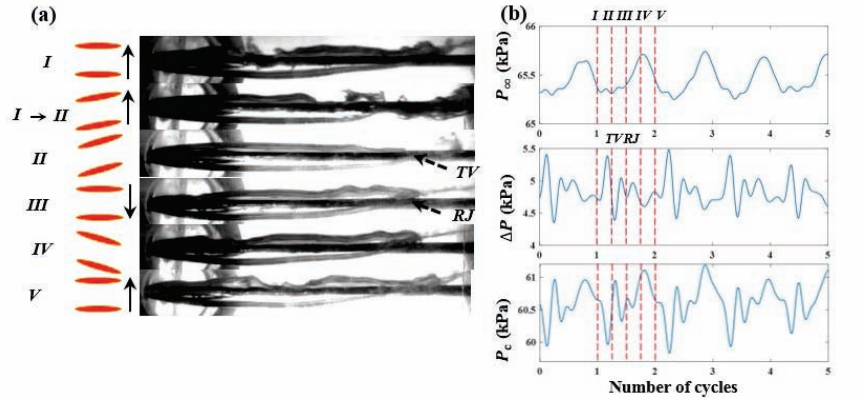


Figure 5. (a) Snapshots showing different phases of supercavity pattern corresponding to different hydrofoil positions in a gust cycle and (b) variation of $P_\infty$ , $\Delta P$ and $P_c$ derived from $P_\infty$ and $\Delta P$ at pulsating state II. The arrows in (a) indicate the motion of hydrofoils.

Pulsating state II is observed under *AoA* 8° with $f_g$ of 5 and 6 Hz. Although the supercavity shows similar pulsating behavior as that in pulsating start I (figure 5(a)), $\Delta P$ displays a sharp spike followed by multiple wavelets in every gust cycle (figure 5(b)). The sharp spike results in a series of higher order spectral peaks in the corresponding PSD of the pressure signal in the frequency range above $2f_g$. Moreover, unlike pulsating state I, the spike in $\Delta P$ displays a 0.13 s delay with respect to Phase III of the hydrofoils when they are moving downward from their neural position. Similar to that in the wavy state, the signal delay matches the time required for the vertical perturbation propagating to the location where the supercavity sheds off air pockets, indicating the cavity pulsation at this state is dictated by the vertical velocity perturbation induced by the hydrofoils rather than the pressure fluctuation associated with varying blockage in pulsating state I. In addition, the variation of cavity length during pulsation (***I→II*** in figure 5(a)) is more drastic compared to that in pulsating state I (***II→III*** in figure 4(a)), which results in the abrupt drop of $P_c$ (i.e., the spike in $\Delta P$). Noteworthily, different from the previous state, the pulsation of the cavity in each gust cycle is always initiated from the upper surface since it is more susceptible to the KH instability due to the gravity effects**.**

Figure 6. A snapshot of the supercavity under collapsing state.

At the highest *AoA* (i.e., *AoA* 10°) and $f_g$ above 2 Hz, the supercavity eventually collapses under a fixed ventilation rate and tunnel speed. At this state, the unsteadiness induced by the gust generator is so strong and rapid such that the supercavity does not have sufficient time to recover through ventilation after its breakup. Note that the reliable pressure measurements cannot be obtained due to water splashing near cavity pressure tap.

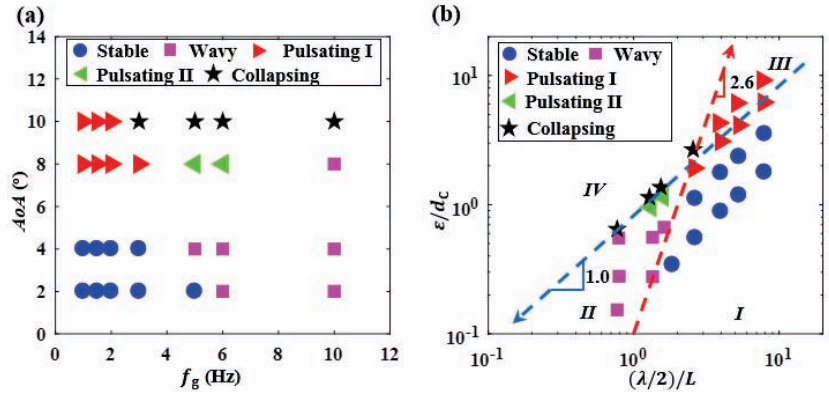


Figure 7. (a) The supercavity state map over a broad range of $f_g$ and *AoA*, and (b) $(\lambda/2)/L$ and $\varepsilon/d_C$ with *Fr*=26.5 and $C_{Qs}$=0.19.

The transition across different supercavity states under a broad range of unsteady conditions is summarized in the supercavity state map (figure 7). As shown in figure 7(a), with fixed $f_g$, the increase of *AoA* enhances the amplitude of the pressure fluctuation in a gust cycle, leading to the pulsating and eventually the collapsing of the supercavity. Similarly, under fixed *AoA*, increasing $f_g$ amplifies the vertical velocity perturbation which results in augmenting the waviness of in the cavity geometry (i.e., stable to wavy, pulsating I to II). To further elucidate the key trends in the supercavity state transition, the state map is also presented with half wavelength $(\lambda/2)$ and wave amplitude $(\varepsilon)$, normalized by the cavity length under steady condition ($L$) and cavitator diameter ($d_C$) in logarithm scale, respectively (figure 7(b)). The non-dimensionalization of wave parameters is intended to compare the perturbation produced from the gust generator with the characteristic length scales of the supercavity. Two dashed lines, termed as critical unsteady condition lines in figure 7(b), are generated by least square fitting of the data points at the border demarcating different cavity states, which divide the map into four regions of different state. The blue dashed line with the arrow represents a dominant effect of wave amplitude (i.e, power index of 2.6) that leads to the supercavity collapsing, while moving along the red line in the direction of the arrow shows a substantial effect of decreasing wavelength that causes cavity to collapse through pulsating states. Moreover, in Region I, the supercavity is stable due to the limited effect of flow

unsteadiness in terms of both the amplitude and wavelength of the perturbations. When the scale of wavelength (precisely, half wavelength) is comparable with the cavity length (i.e, $(\lambda/2)/L{\sim}1$) under limited amplitude (i.e., $\varepsilon/d_C < 1$), the cavity enters into wavy state in Region II. Comparatively, when wave amplitude increases above the characteristic lateral scale of the cavity (i.e., $\varepsilon/d_C > 1$) with limited longitudinal perturbation characterized by the wavelength, the cavity transition to pulsating state I (Region III). The supercavity collapsing (Region IV) can be achieved when both the amplitude and the wavelength of the perturbations become sufficiently strong (i.e., $(\lambda/2)/L \lesssim 1$ and $\varepsilon/d_C > 1$).

## Conclusion

Five distinct states (stable state, wavy state, pulsating state I, pulsating state II and collapsing state) are observed in a systematic investigation of cavity behaviors in the unsteady flow. We attribute different cavity behaviors under varying unsteady conditions to the effects of vertical perturbation induced by gust generator motion and/or pressure fluctuation caused by varying blockage. The cavity state map suggests that the cavity states is dependent on the characteristic scale (i.e., half wavelength and wave amplitude) of the perturbation comparing to the cavity dimension. Future investigation will be focused on the influence of ventilation conditions (e.g., ventilation rate and cavitator size) on the cavity behaviors.

## References

[1] Nesteruk, I. (2012). *Supercavitation*. Springer-Verlag, Berlin Heidelberg.
[2] Logvinovich, G. V. (1969) *Hydrodynamics of flows with free boundaries* Naukova Dumka, Kiev. ch.5.
[3] Semenenko, V.N. (2001) Artificial supercavitation: physics and calculation. Ukrainian academy of sciences, Kiev Institute of hydromechanics.
[4] Lee, S.J., Kawakami. E., Arndt, R.E.A. (2013). *Investigation of the behavior of ventilated supercavities in a periodical gust flow.* Journal of Fluid Engineering. 135(8).
[5] Karn, A., Arndt, R.E.A., Hong, J. (2015). *Dependence of supercavity closure upon flow unsteadiness.* Experimental Thermal and Fluid Science. 68.
[6] Karn, A., Arndt, R.E.A., Hong, J. (2016a). *Gas entrainment behavior in the formation and collapse of a ventilated supercavity.* Experimental Thermal and Fluid Science. 79.
[7] Karn, A., Arndt, R.E.A., Hong, J. (2016b). *An experimental investigation into supercavity closure mechanisms.* Journal of. Fluid Mechanics, 789.
[8] Shao, S., Karn, A, Ahn, B-K., Arndt, R.E.A., Hong, J. (2017). *A comparative study of natural and ventilated supercavitation across two closed-wall water tunnel facilities.* Experimental Thermal and Fluid Science. 88.
[9] Jiang, Y., Shao, S., Hong, J. (2018). *Experimental investigation of ventilated supercavitation with gas jet cavitator.* Physics of Fluids, 30.
[10] Korpriva, J., Arndt, R.E.A., Amromin. E.L. (2008). *Improvement of hydrofoil performance by partial ventilated cavitation in steady flow and periodic gusts.* Journal of Fluid Engineering. 130(3).
[11] Newman, J. N. (1977). *Marine hydrodynamics.* The MIT Press, Cambridge, MA.
[12] Chandrasekhar, S. (1961). *Hydrodynamic and hydromagnetic stability.* Dover Publications, NY.